

Eccentricity Driven Climate Effects in the Kepler-1649 System

STEPHEN R. KANE,¹ ZHEXING LI,¹ ERIC T. WOLF,² COLBY OSTBERG,¹ AND MICHELLE L. HILL¹¹*Department of Earth and Planetary Sciences, University of California, Riverside, CA 92521, USA*²*Laboratory for Atmospheric and Space Physics, Department of Atmospheric and Oceanic Sciences, University of Colorado, Boulder, CO, USA*

ABSTRACT

The discovery of terrestrial exoplanets is uncovering increasingly diverse architectures. Of particular interest are those systems that contain exoplanets at a variety of star–planet separations, allowing direct comparison of exoplanet evolution (comparative planetology). The Kepler-1649 system contains two terrestrial planets similar both in size and insolation flux to Venus and Earth, although their eccentricities remain largely unconstrained. Here we present results of dynamical studies of the system and the potential effects on climate. The eccentricities of the Kepler-1649 system are poorly constrained, and we show that there are dynamically viable regions for further terrestrial planets in between the two known planets for a limited range of eccentricities. We investigate the effect of eccentricity of the outer planet on the dynamics of both planets and show that this results in high-frequency (1000–3000 years) eccentricity oscillations in long-term stable configurations. We calculate the resulting effect of these eccentricity variations on insolation flux and present the results of 3D climate simulations for the habitable zone planet. Our simulations demonstrate that, despite large eccentricity variations, the planet can maintain stable climates with relatively small temperature variations on the substellar hemisphere for a variety of initial climate configurations. Such systems thus provide key opportunities to explore alternative Venus/Earth climate evolution scenarios.

Keywords: astrobiology – planetary systems – planets and satellites: dynamical evolution and stability
– stars: individual (Kepler-1649)

1. INTRODUCTION

Over the past several decades, thousands of exoplanets have been discovered enabling statistical studies of exoplanet occurrence rates (Catanzarite & Shao 2011; Dressing & Charbonneau 2015; Kopparapu 2013; Winn & Fabrycky 2015). These studies include the investigation of planets that lie within the Venus Zone (VZ) (Kane et al. 2014) and Habitable Zone (HZ) (Kasting et al. 1993; Kane & Gelino 2012; Kopparapu 2013; Kopparapu et al. 2014; Kane et al. 2016). A primary purpose of such studies is to place our solar system within the context of planetary system architectures. One aspect of this context is determining the frequency of systems that have terrestrial planets in both the VZ and HZ. Such systems may provide potential analogs for Venus and Earth, that in turn may provide key in-

sights into the divergence of the Venus/Earth atmospheric evolutions (Kane et al. 2019; Ostberg & Kane 2019). Examples of such systems include TRAPPIST-1 (Gillon et al. 2016, 2017; Luger et al. 2017), LHS 1140 (Dittmann et al. 2017; Ment et al. 2019), and Kepler-186 (Quintana et al. 2014). Amongst the factors that influence the climate evolution of terrestrial exoplanets are the eccentricity variations (Barnes et al. 2013; Way & Georgakarakos 2017), which may have contributed to the water loss of Venus (Kane et al. 2020b). Thus, a pathway to understanding the major factors behind the Venus/Earth divergence is exploring the dynamical impacts of eccentricity variations that may have occurred (and continue to occur) in exoplanetary systems.

A particularly strong contributor to the currently known inventory of terrestrial exoplanets was the *Kepler* mission (Borucki et al. 2010), from which a catalog of HZ planets was constructed (Kane et al. 2016). The Kepler-1649 system was discovered by Angelo et al.

(2017) which identified the observed planet as a potential Venus analog due to the planetary size and similarity of insolation flux to that of Venus. The prospect of the planet as a Venus analog was strengthened by the detailed climate simulations of Kane et al. (2018), that showed the rapid rise in surface temperature from a variety of initial conditions. The system became a strong comparative planetology target when a further terrestrial planet was discovered in the HZ by Vanderburg et al. (2020). Thus, Kepler-1649 has joined a select group of systems that are known to harbor terrestrial planets in both the VZ and HZ. This class of system also provides opportunities to study the role of complex dynamical evolution on the orbital variation of planets (Smith & Lissauer 2009; Petrovich 2015), including those within the HZ (Kopparapu & Barnes 2010; Kane 2015; Kane et al. 2020a).

In this paper we present a dynamical and climate study of the Kepler-1649 system, describing the potential eccentricity variations that result from the interactions between the planets, and the possible impact on the climate of the HZ planet. Section 2 describes the architecture of the system, provides estimates for the planetary masses, and places constraints on the presence of additional planets. Section 3 presents the results of dynamical simulations that explore the amplitude and frequency of eccentricity cycles through angular momentum exchanges between the planets. The consequences of these dynamical interactions are discussed in Section 4, including climate models of the surface temperatures for various eccentricities and ocean models. These climate simulations are provided for distinct eccentricities for Kepler-1649c, which represent relatively short-lived climate states for high-frequency eccentricity oscillations. We provide a discussion of the results, their implications, and concluding remarks in Section 5.

2. SYSTEM ARCHITECTURE

As described in Section 1, the Kepler-1649 system is particularly fascinating from a comparative planetology aspect, since it contains both potential analogs to Venus and Earth within the same system. The stellar properties provided by Vanderburg et al. (2020) include the mass ($M_\star = 0.1977 \pm 0.0051 M_\odot$), radius ($R_\star = 0.2317 \pm 0.0049 R_\odot$), luminosity ($L_\star = 0.00516 \pm 0.00020 L_\odot$), and effective temperature $T_{\text{eff}} = 3240 \pm 61$ K). The radii of the known planets in the system are $R_p = 1.017 \pm 0.051 R_\oplus$ and $R_p = 1.06^{+0.15}_{-0.10} R_\oplus$ for planets b and c respectively. To calculate the semi-major axes of the planets, a , we use the a/R_\star information provided by Vanderburg et al. (2020), resulting in semi-major axes of 0.0482 ± 0.0010 AU and 0.0827 ± 0.0017 AU for plan-

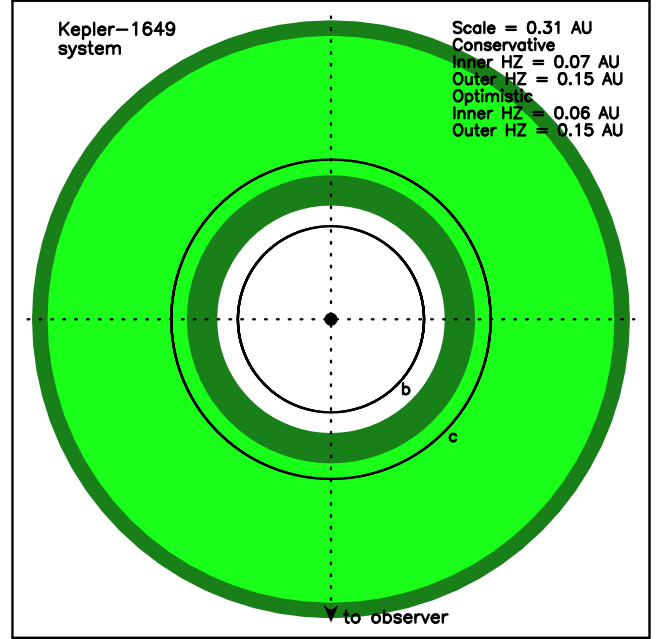


Figure 1. A top-down view of the Kepler-1649 system, where the star location is at the center of the crosshairs and the orbits of the known planets are indicated by solid circles. The extent of the CHZ is shown as the light green region and the OHZ extension to the CHZ is shown as the dark green region.

ets b and c respectively. The conservative HZ (CHZ) boundaries are defined by the runaway greenhouse limit at the inner edge and the maximum greenhouse limit at the outer edge. The optimistic HZ (OHZ) boundaries are determined empirically based on the assumption that Venus may have had surface liquid water as recently as 1 Gya, and that Mars may have surface liquid water ~ 3.8 Gya. These boundaries are described in more detail by Kane et al. (2016); Kane (2018). Based on the above system properties, we calculated the extent of the CHZ and OHZ boundaries for Kepler-1649 as 0.075–0.147 AU and 0.059–0.155 AU respectively. The outer edge of the VZ corresponds to the inner edge of the CHZ (the runaway greenhouse limit) at 0.075 AU. The extent of the HZ and the orbits of the planets are represented in Figure 1.

Although the orbits of the planets are shown as circular in Figure 1, Vanderburg et al. (2020) do not constrain the eccentricities in any significant way, though smaller planets tend to have small eccentricities (Kane et al. 2012). Vanderburg et al. (2020) further suggested that there could be an additional planet in an orbit that lies between the two known planets. This suggestion was partially motivated within the context of mean motion resonances (MMR) that may exist within the system. The known b and c planets are close

to the 9:4 MMR, which is a relatively weak resonance in terms of planetary perturbations. However, an additional planet between the known planets at a location of ~ 0.063 AU would create a 3:2 resonant chain with high stability potential (Batygin & Morbidelli 2013). Furthermore, an analysis of Kepler systems by Weiss et al. (2018) found that planetary architectures may preferentially contain similar sized planets (Millholland et al. 2017), with the vast majority of Kepler planets having a spacing greater than 10 mutual Hill radii. Assuming an Earth mass for all three planets, a planet located at the 3:2 resonant chain location between planets b and c would be ~ 12.5 mutual Hill radii away from either planet, consistent with the observed spacings in other Kepler systems.

To investigate the prospect of an additional planet as a function of eccentricity, we conducted a dynamical simulation using the REBOUND orbital dynamics package (Rein & Liu 2012). Such an investigation requires an estimate of the planetary masses. There are numerous planetary mass-radius relationships that have been developed from which such an estimate may be derived (e.g., Kanodia et al. 2019; Zeng et al. 2019; Neil & Rogers 2020; Otegi et al. 2020; Turbet et al. 2020). For our dynamical simulations, we adopt the mass estimates provided by the FORECASTER tool (Chen & Kipping 2017), which produces mass estimates of $1.06 M_{\oplus}$ and $1.21 M_{\oplus}$ for planets b and c respectively.

The dynamical simulation was carried out using the Mean Exponential Growth of Nearby Orbits (MEGNO) package within REBOUND with the symplectic integrator WHFast (Rein & Tamayo 2015). MEGNO is a chaos indicator that is useful in dynamical simulations to distinguish the quasi-periodic or chaotic orbital time evolution of planetary systems. The final numerical value returned by a MEGNO simulation indicates whether the system would end up in a chaotic state or not, where a chaotic state is less likely to maintain long-term stability. For our simulation, we explored the possibility of an additional planet in between the orbits of planet b and c by testing how varying eccentricity and semi-major axis values for an injected planet of one Earth mass affects the stochasticity of the system. We conducted four sets of simulations that varied eccentricity, each providing a grid of orbital parameters for the injected planet’s eccentricity (0.0–0.3) and semi-major axis (0.0482–0.0827 AU). Since the eccentricities of the two known planets are unconstrained, we tested planet b and c eccentricities of 0.0, 0.1, 0.2, and 0.3. Each simulation duration was 10 million orbits for the outer most planet with a time step of 0.001 years (0.365 days). The

integration was set to stop and return a large MEGNO value if the planet was ejected beyond 100 AU. The results of our simulations for all four eccentricity cases are shown in the top four panels of Figure 2. The axes indicate the semi-major axes and eccentricities tested for the injected planet in each of the four cases. The colors correspond to the final MEGNO value for each specific combination, with a MEGNO value ~ 2 (green) indicating a non-chaotic system (Hinse et al. 2010) and quasi-periodic motion for all planets. A high MEGNO result, shown as red, indicates high chaos, and irregular events that cause an early termination of the simulation, such as close encounters and collision events, are shown in white. The four simulations described above assumed an argument of periastron for all three planets of 90° . We conducted further simulations that varied the argument of periastron of the injected planet with respect to those of the known planets. The results of these simulations for the eccentricity 0.1 and 0.3 cases (for all planets) are shown in the bottom two panels of Figure 2.

As can be seen in the top four panels of Figure 2, there is a large parameter space between approximately 0.052 AU and 0.075 AU with low eccentricity values where the injected Earth-mass planet could be located with long-term stability. The largest range of eccentricities for the injected planet that allow a stable configuration occur at 0.063 AU which, as stated above, is the location of the 3:2 MMR chain. The additional spikes visible in the stability distribution, most obvious in the top-left panel, also correspond to MMR locations, such as the 5:4 resonance location at ~ 0.071 AU. However, as the eccentricities for both planet b and c increase to higher values, the stable locations for the injected planet indicated by the green color gradually diminishes and the locations shift to higher eccentricity values. When the eccentricities for both planet b and c exceed 0.3, the stable locations for the injected planet vanish, the reasons for which are discussed in Section 3. The bottom two panels of Figure 2 show that, even for the eccentricity case of 0.1 (bottom-left), the system is most stable when the pericenters of the planets are approximately aligned. As seen in the bottom-right panel of Figure 2, the scarce regions of stability for the eccentricity case of 0.3 matches the relative instability seen in the middle-right panel. It is worth noting that the described simulations assumed system coplanarity, and the introduction of mutual inclinations may present additional regions of stability, particularly for scenarios that mitigate potential overlap of orbits.

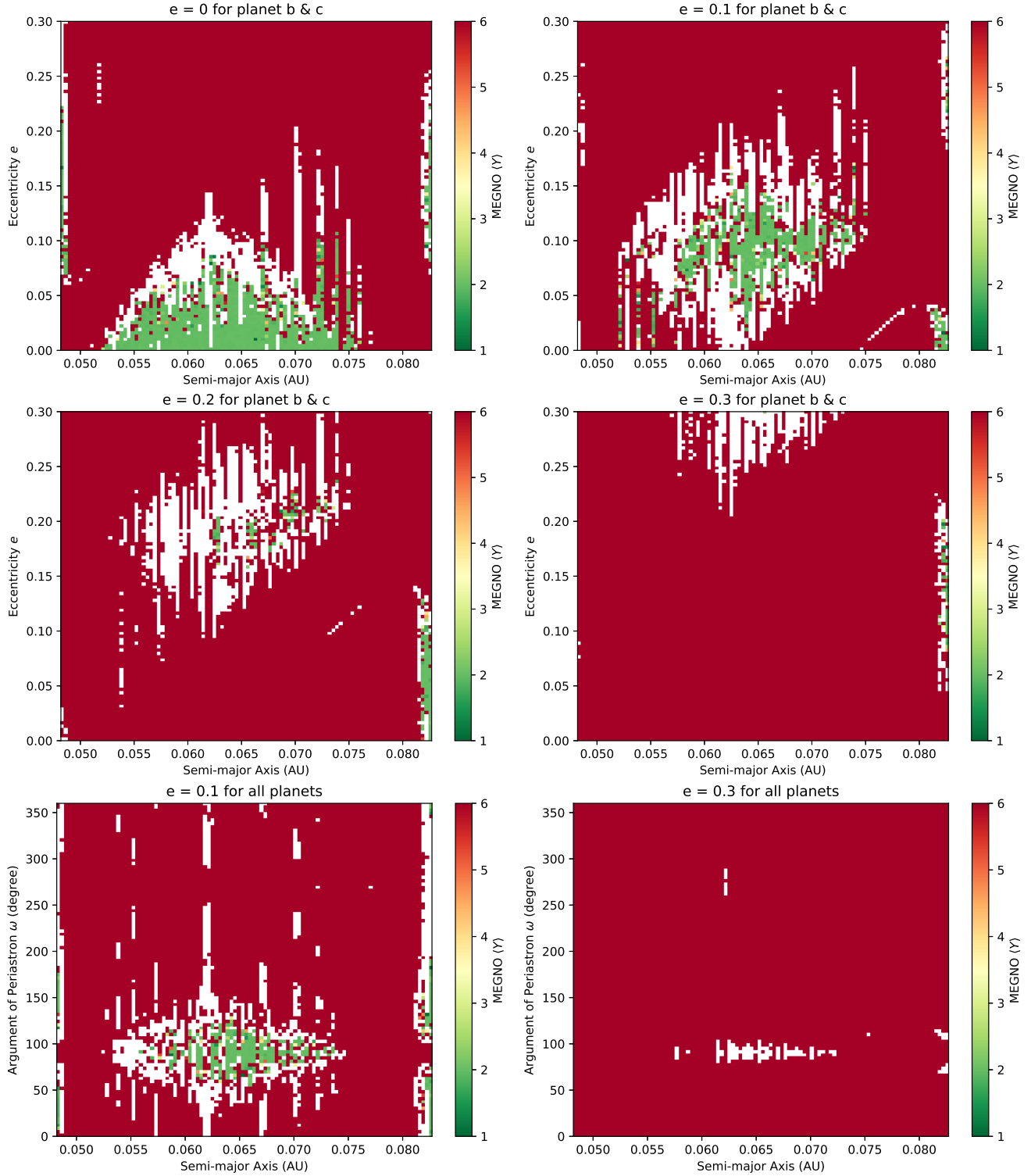


Figure 2. Results of a MEGNO analysis of the system, exploring the viability of an additional terrestrial planet in between planets b and c. This analysis was performed assuming initial eccentricities for planets b and c of 0.0 (top-left), 0.1 (top-right), 0.2 (middle-left), and 0.3 (middle-right). The color scales indicate the final MEGNO value from the simulations, where green represents a stable system configuration, red represents an unstable (chaotic) system, and white represents an early termination of the simulation. Shown in the bottom panels are simulations that vary the argument of periastron for the injected planet for eccentricities of 0.1 (bottom-left) and 0.3 (bottom-right).

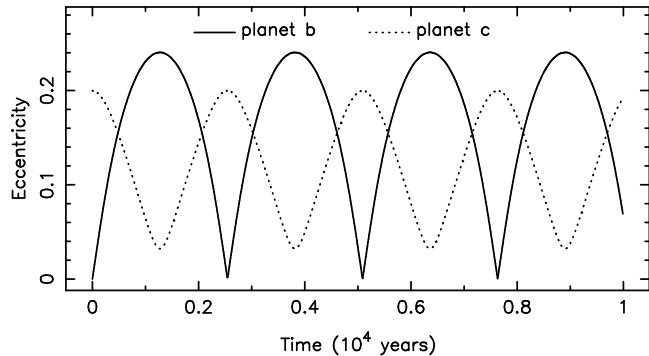


Figure 3. Eccentricity as a function of time for planet b (solid line) and planet c (dotted line) for the case of FORECASTER planet masses ($1.06 M_{\oplus}$ and $1.21 M_{\oplus}$ respectively) and a starting eccentricity for planet c of 0.2.

3. ECCENTRICITY INDUCED DYNAMICAL CYCLES

As demonstrated in Section 2, a non-zero eccentricity for the known planets can place significant restrictions on the presence of an additional terrestrial planet between them. Here we investigate the time-dependent dynamical effects of non-zero eccentricities. Such investigations have been carried out in numerous other works in a more general context (Gladman 1993; Chambers et al. 1996; Hadden & Lithwick 2018). Our N-body integrations were performed with the Mercury Integrator Package (Chambers 1999), adopting a similar methodology to that described by Kane & Raymond (2014); Kane (2016, 2019). The simulations used a hybrid symplectic/Bulirsch-Stoer integrator with a Jacobi coordinate system to provide increased accuracy for multi-planet systems (Wisdom & Holman 1991; Wisdom 2006). The time resolution of the simulations was set to 0.2 days in order to comply with the recommendations of Duncan et al. (1998) that require resolutions be $1/20$ of the shortest orbital period (8.69 days for planet b).

We performed a series of dynamical simulations using the above criteria that explore a range of eccentricities. Specifically, we started each simulation with a circular orbit for planet b and eccentricities for planet c that ranged from 0.0 to 0.5 in steps of 0.05. Each simulation was allowed to run for 10^6 years, or $\sim 1.8 \times 10^7$ orbits of planet c, with orbital parameters for both planets output every 10 simulation years. The suite of simulations that explored the full range of starting eccentricities for planet c were conducted using Earth masses for both planets b and c, and also using the FORECASTER masses described in Section 2.

The full set of dynamical simulations demonstrated that the system is able to remain stable for 10^6 years

up to a starting eccentricity for planet c of 0.325, beyond which the system rapidly loses dynamical integrity. The 0.325 eccentricity upper limit was true for both the Earth-mass and FORECASTER-mass scenarios. In particular, we found that the eccentricity of planet c induces a near-equivalent eccentricity in planet b, whereby each planet oscillates in eccentricity in order to conserve the system angular momentum. For example, shown in Figure 3 are the time-dependent eccentricities of planet b (solid line) and planet c (dotted line) where the assumed masses are those from FORECASTER and the starting eccentricity of planet c is 0.2. The figure demonstrates the full amplitude and frequency of the eccentricity variations over a relatively brief period of 10^4 years. The period of the eccentricity oscillations in this case is ~ 2500 years.

To investigate this further, we conducted a fourier analysis of each of the dynamical simulation outputs described above. The periods of the eccentricity oscillations, for both FORECASTER and Earth masses, as a function of starting planet c eccentricity are shown in Figure 4. There are several aspects to note about this figure. Firstly, the period of the oscillations decreases with increasing eccentricity. Secondly, the period of the oscillations is systematically smaller for the larger FORECASTER masses. Thirdly, the dynamical instability that results beyond eccentricities of 0.3 is clearly visible and is likely related to the diminishing oscillation period with increasing eccentricity. These simulation results agree well with similar calculations that may be performed using the analytical expressions derived by Hadden & Lithwick (2018). It is worth noting that the period of the eccentricity oscillations and the eccentricity at which instability occurs is likely influenced by the proximity of the planets to the 9:4 MMR (Vinson & Chiang 2018; Hadden 2019), discussed in Section 2. Additional factors include the mutual inclinations of the planets combined with non-zero stellar obliquity (Spalding et al. 2018). Regardless, the high frequency of eccentricity oscillations may result in significant climate consequences for the planets.

4. DYNAMICAL CONSEQUENCES ON CLIMATE

Here we discuss the implications of the variable eccentricity for the possible climate scenarios of planet c. Given the system parameters provided in Section 2, the insolation flux received by planet c at its semi-major axis is $\sim 75\%$ of the mean Earth insolation flux. The eccentricity oscillations described in Section 3 will result in a correspondingly variable insolation flux for the planet, whose amplitude and period depend on the eccentricity. For example, consider the case of a starting eccentricity

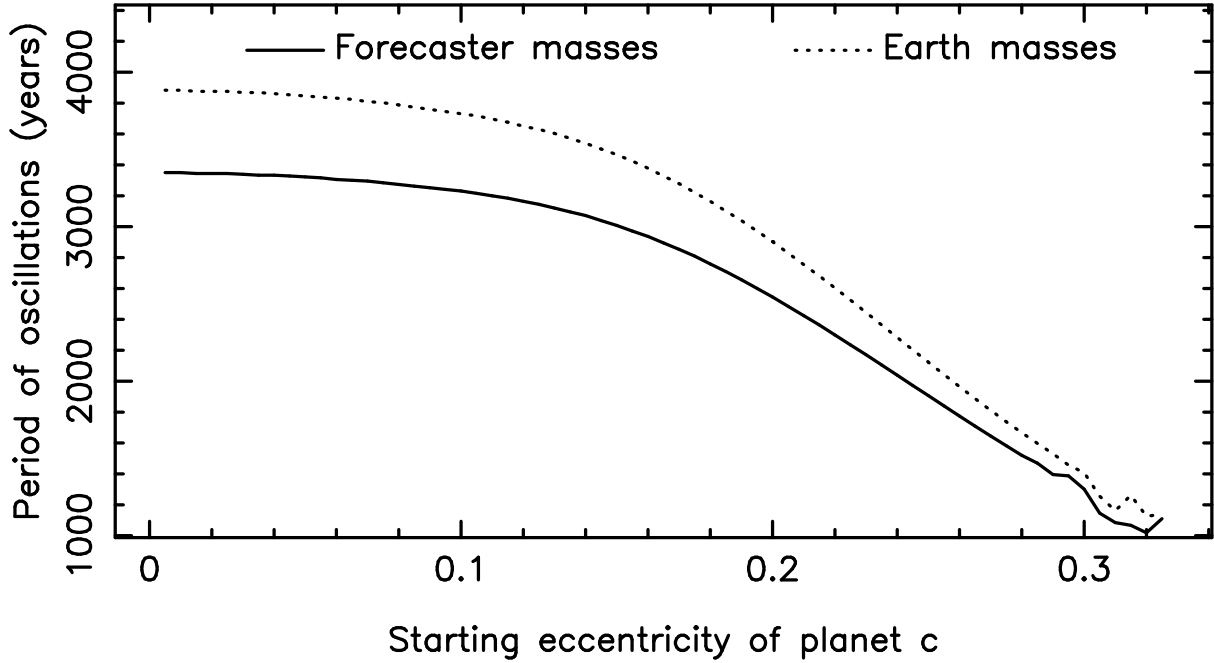


Figure 4. The period of the eccentricity oscillations of planets b and c as a function of the starting eccentricity for planet c, for both the FORECASTER-mass (solid line) and Earth-mass (dotted line) cases. Note that the system is dynamically unstable for eccentricities beyond ~ 0.3 .

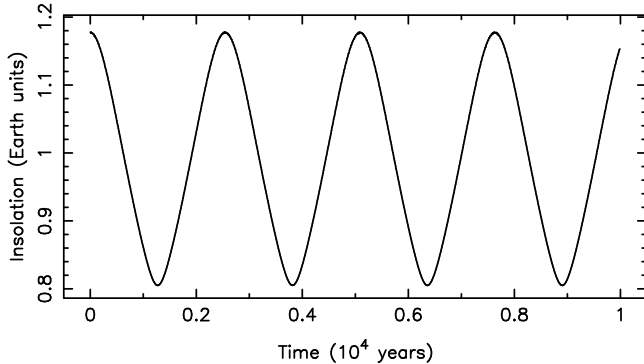


Figure 5. Maximum flux (insolation) received by planet c during a single orbit (in Earth units) as a function of time for an eccentricity of 0.2.

of 0.2 for planet c, as shown in Figure 3. The variation in the maximum insolation flux of the planet with time is shown in Figure 5. Since, as shown in Figure 3, the eccentricity of planet c never reaches zero, the maximum insolation flux is always larger than that for a circular orbit. Figure 5 shows that the maximum insolation in this case oscillates approximately around an Earth equivalent flux with a variation of $\pm 20\%$.

The Resolving Orbital and Climate Keys of Earth and Extraterrestrial Environments with Dynamics (ROCKE-3D), described in detail by Way et al. (2017), is a three-dimensional climate system model developed at the NASA Goddard Institute for Space

Studies (GISS) specifically for studying planetary and exoplanetary atmospheres. We use ROCKE-3D to constrain the climatic effects of oscillations in the orbital-rotational properties of Kepler-1649c. ROCKE-3D has previously been used for studying the climate and habitability of terrestrial extrasolar planets, including studies of Proxima Centauri b (Del Genio et al. 2019), moist and runaway greenhouse states (Fujii et al. 2017; Way et al. 2018; Kane et al. 2018), the effects of planet orbital-rotational properties (Way & Georgakarakos 2017; Colose et al. 2019), and the effects of ocean circulation (Checlair et al. 2019; Olson et al. 2020; Salazar et al. 2020). While the atmospheric composition and surface properties of Kepler-1649c remain unconstrained, here we have conducted a set of simulations using ROCKE-3D to illuminate the possible role of eccentricity evolution on climate. Following from Figure 4, for a starting eccentricity of 0.3, Kepler-1649c could experience eccentricity oscillations on ~ 1200 year timescales. To constrain the bounds of the potential climate states experienced by Kepler-1649c during its dynamical evolution, we simulate scenarios with zero eccentricity and synchronous rotation, and with an eccentricity of 0.3 and a 3:2 resonant rotation state. Note, for these cases we are not simulating the continuous evolution of Kepler-1649c over many thousands of years, but rather we are simulating the equilibrium climate states for potential end-member orbital-

rotational configurations. However, if the spin dynamics become chaotic, these end-member rotation states may not be fully realized (Correia & Laskar 2004). Thus, we also conduct simulations that assume a constant, non-resonant asynchronous spin rate in order to approximate chaotic spin dynamics. For these cases, we assume a 16 Earth-day rotation period, which is an intermediate value between the synchronous rotation period of ~ 19.535 days, and the 3:2 resonant rotation period of ~ 13.0235 days. Each of our simulations achieve radiative equilibrium after 100–200 years, well within the timescales of possible eccentricity variations described in Section 3. This is also comparable to the timescales provided by the continuously variable eccentricity approach adopted by Way & Georgakarakos (2017).

As described in Section 2, Kepler-1649c lies within the CHZ, close to the inner edge. In all climate simulations conducted here we assume a globally ocean covered planet with no emergent continents. While this represents only one of many potential surface configurations for Kepler-1649c, the study of ocean covered worlds provides a first-order approximation for the study of climate evolution on potentially habitable worlds. We test two different assumptions for the ocean layer. "Slab" ocean simulations assume a 100 m deep ocean layer with no horizontal transports, but with the thermodynamic exchange of heat and moisture between the ocean and atmosphere. "Dynamic" ocean simulations utilize a 900 m deep fully coupled ocean circulation model capable of predicting horizontal and vertical transports, in addition to thermodynamic exchanges with the atmosphere. Both ocean configurations allow for sea-ice formation. Salinity is held equal to that of the modern Earth's ocean. Atmospheric compositions also remain unconstrained from observations and therefore constitute a large uncertainty on the climate state. Here, we choose two nominal atmospheric compositions which are "Earth-like" (1 bar total with 400 ppm CO_2 and an N_2 background), and a 1 bar CO_2 atmosphere. For all climate simulations, water vapor and clouds are variable constituents in the atmosphere, controlled by temperature, evaporation, convection, advection, and condensation. Our selections for atmospheric compositions were taken from the test cases for habitable exoplanets proposed by Fauchez et al. (2020), that facilitate the study of a diversity of climate states. For planets residing in the middle of the habitable zone, as does Kepler-1649c, an Earth-like atmospheric composition will result in a cold climate state, dominated by ice and where ocean transport processes are of particular importance (Del Genio et al. 2019), while a 1 bar CO_2 atmosphere will result in a warm climate state, dominated by the

hydrological cycle, clouds, and atmospheric transport (Yang et al. 2019). Thus the selection of these two atmospheric compositions allows us to capture some diversity of habitable zone climates. A wide ranging parameter study of the infinite variety of possible surface and atmospheric compositions for Kepler-1649c is beyond the scope of this work. In total, we have conducted 16 different climate simulations of Kepler-1649c, with results summarized in Table 1.

Figure 6 shows surface temperature maps from our climate simulations with ROCKE-3D. The results shown are from an average of the last 100 orbits of Kepler-1649c (i.e. 1950 Earth days, 5.3 Earth years). The bold white line indicates where the surface temperature is 273 K, and thus serves as a close proxy for the sea ice margin. The columns show climate results from different rotation states, including synchronous, resonant, and chaotic. Synchronous rotation assumes zero eccentricity and a rotation period equaling the orbital period. Resonant rotation assumes a rotation period in a 3:2 resonance with the orbital period and an eccentricity of 0.3. Chaotic rotation, as mentioned previously, is approximated by a 16 day asynchronous rotation period. The global mean surface temperature and surface temperature maps are largely unchanged for chaotic rotators with eccentricities of zero or 0.3. Thus, plotted are an average between these two states. Finally, each row in figure 6 illustrates different atmosphere and surface combinations, including Earth-like and 1 bar CO_2 atmospheres, with slab and dynamic ocean models.

Global mean surface temperatures range between 244.7 K and 304.8 K, and surface liquid water is maintained over at least some of the planet surface in all of the cases simulated (Table 1). Thus, all climates simulated are at least partially habitable, with many states being globally habitable. If the orbital-rotational state of Kepler-1649c can fully oscillate between synchronous and resonant modes, significant temporal changes to the global mean surface temperatures and the total habitable area of the planet, which here we use the open ocean fraction as a proxy for the habitable surface area, would occur. The shift from synchronous rotation to resonant rotation affects climate both by changing the longitudinal patterns of the stellar flux incident on the planet, and also by changing the Coriolis parameter which feeds back on atmospheric and ocean circulations. The breaking of synchronicity and the increase in the rotation rate tends to result in increased zonal transports resulting in longitudinally banded patterns, as opposed to the classic eyeball climate states found for slow and synchronous rotators (Pierrehumbert 2011; Turbet et al. 2016; Kopparapu et al. 2017; Haqq-Misra et al. 2018).

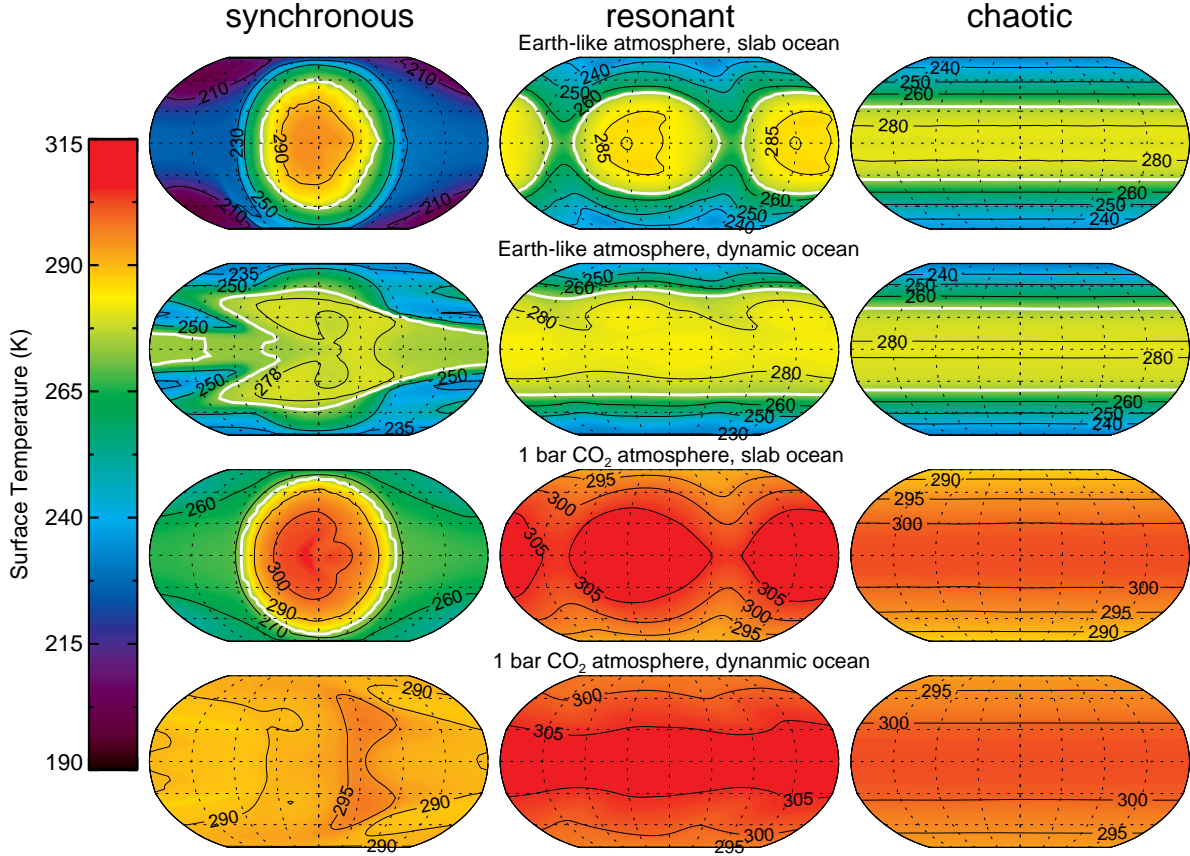


Figure 6. Surface temperatures maps from our climate simulations of Kepler-1649c. The left column assumes synchronous rotation with zero eccentricity, the center column assumed 3:2 resonant rotation with an eccentricity of 0.3, and the right column assumes chaotic rotation approximated by a 16 day asynchronous orbit. For the chaotic states, eccentricity does not have a significant effect on the climate and thus zero and 0.3 eccentricity results are averaged together. Rows (labeled) illustrate the different surface and atmospheric configurations. All simulations were performed with ROCKE-3D.

The inclusion of non-zero eccentricity with a 3:2 orbital resonance produces a characteristic double hot-spot evident in temporal mean climate statistics, due to the fact that two opposite faces of the planet are periodically irradiated at perihelion (Boutle et al. 2017; Del Genio et al. 2019). The double hot spot pattern is clearly evident in the slab ocean cases. The orbital period of Kepler-1649c is short (19.5 days) compared to thermal timescales of the ocean, thus opposing sides of the planet remain permanently warm. For dynamic ocean cases, a faint signal of the double hot spot phenomenon persists, but zonal heat transports by the ocean results in nearly zonally uniform patterns of surface temperature (Figure 6).

For corresponding end-member scenarios of synchronous and resonant modes (Table 1), global mean surface temperatures could change by as little as 8.9 K for an Earth-like atmosphere with dynamic ocean circulation or by as much as 28.4 K for a CO₂ dominated planet with a slab ocean. For both atmospheric com-

positions, the climate sensitivity between end-member orbital-rotational states is reduced when considering a full dynamic ocean compared to the slab ocean cases. Perhaps surprisingly, the optically thicker 1 bar CO₂ simulations are more sensitive to the orbital-rotational state than are the Earth-like atmosphere. While further investigation is warranted, we surmise that this is due to more vigorous water vapor and cloud feedbacks that occur for our 1 bar CO₂ atmospheres, due to their generally warmer climate states compared to the Earth-like atmospheres which remain cold and ice dominated.

However, as noted above, these end-member scenarios may never be fully realized. The relatively rapid changes in orbital-rotational states may instead drive Kepler-1649c into chaotic rotation, which would result in asynchronous planet rotation and not into any favored resonant state. In such a scenario, the climate patterns of Kepler-1649c become zonally uniform for all combinations of atmospheric composition and ocean assumptions (Figure 6 third column), as starlight would

#	Rotation State	Atmosphere	Ocean	T_S mean (K)	Ocean (%)	Albedo
1	1:1, $e = 0.0$	Earth-like	slab	244.7	25.1	0.303
2	3:2, $e = 0.3$	Earth-like	slab	268.0	57.9	0.223
3	16 day, $e = 0.0$	Earth-like	slab	266.0	61.2	0.199
4	16 day, $e = 0.3$	Earth-like	slab	268.9	70.1	0.215
5	1:1, $e = 0.0$	Earth-like	dynamic	263.4	62.5	0.244
6	3:2, $e = 0.3$	Earth-like	dynamic	272.3	79.2	0.210
7	16 day, $e = 0.0$	Earth-like	dynamic	267.6	68.6	0.187
8	16 day, $e = 0.3$	Earth-like	dynamic	269.6	73.0	0.210
9	1:1, $e = 0.0$	1 bar CO ₂	slab	275.7	39.2	0.239
10	3:2, $e = 0.3$	1 bar CO ₂	slab	304.1	100	0.245
11	16 day, $e = 0.0$	1 bar CO ₂	slab	296.8	100.0	0.258
12	16 day, $e = 0.3$	1 bar CO ₂	slab	301.2	100.0	0.272
13	1:1, $e = 0.0$	1 bar CO ₂	dynamic	291.3	100	0.269
14	3:2, $e = 0.3$	1 bar CO ₂	dynamic	304.8	100	0.246
15	16 day, $e = 0.0$	1 bar CO ₂	dynamic	297.0	100.0	0.262
16	16 day, $e = 0.3$	1 bar CO ₂	dynamic	303.4	100.0	0.262

Table 1. Basic climatic statistics from 3D climate simulations of Kepler-1649c with ROCKE-3D.

irradiate all longitudes of the planet equally with no preferred faces receiving more insolation on time-average than any other.

In all cases simulated, the change in surface temperature caused by the dynamical evolution is relatively small on the substellar hemisphere, but is much larger for the antistellar hemisphere. Here, we define substellar and antistellar hemispheres based on the synchronous rotating orbital-rotational reference frame. Naturally, for non-synchronous cases (resonant and chaotic), all sides of the planet receive periodic stellar flux, meaning that the opposing hemisphere is no longer permanently cloaked in darkness and enjoys its moment in the starlight, resulting in considerable warming. The substellar-antistellar dichotomy is most strongly seen for the slab ocean cases. In both synchronous and resonant rotating instances, the inclusion of dynamic ocean circulations effectively transports heat from the day-side to the night-side of the planet, muting the substellar-antistellar dichotomy.

Our 3D climate simulations reveal that the modulation of orbital-rotational states does not trigger true climate catastrophes for Kepler-1649c (i.e., runaway glaciation or runaway greenhouse states) given the atmospheric compositions explored here. If Kepler-1649c oscillates between synchronous and resonant states, significant millennial scale climate changes would occur that are far in excess of anything that the Earth has experienced over such a short timescale. Given the timescales of variation here (Figure 3), life as we know it may struggle to adapt to such wide temperature vari-

ations indicated by our simulations. Extant lifeforms may remain confined to the substellar hemisphere due to its relative climatic stability compared to the significantly more intense variations that occur on the antistellar hemisphere. However, if instead Kepler-1649c settles into chaotic rotation, millennial scale climate changes would be negligible.

Other factors not explored here may also affect the sensitivity of Kepler-1649c’s climate to oscillations in its orbital-rotational state. Here we have modeled only selected states in equilibrium. If the orbital-rotational state of Kepler-1649c instead evolves monotonically between our illustrated end-member cases, the climate states may instead gradually smear between synchronous and resonant. Chaotic rotation states may also experience time evolution of the rotation period. However, differences in non-resonant asynchronous rotation periods are not likely to drive significant changes in climate, compared to toggling into, and out of, synchronous and resonant states.

The atmospheric composition also presents a significant unconstrained parameter. While the atmospheric compositions studied here all result in temperate climates, if the atmosphere of Kepler-1649c were considerably different, the climate sensitivity between states may deviate considerably. For instance, if Kepler-1649c possesses an overwhelmingly dense, cloud and haze filled atmosphere, the surface may receive little direct starlight and become decoupled from changes in the patterns of stellar flux, and surface temperatures may trend toward a globally uniform state regardless of rotation state

(Turbet et al. 2016). Alternatively, if Kepler-1649c instead has a dry, clear, optically transparent atmosphere, the change in rotation state may also cause little difference to the surface temperature as the planet’s energy balance and thus climate would be governed simply by the albedo and emissivity properties of the planet’s solid surface, along with the instantaneous stellar flux input. Finally, our results indicate that the ocean treatment makes a considerable difference in the modulation of surface temperatures between synchronous and resonant states, but makes little difference for the chaotic rotation state. Still, changes in the ocean depth, and the presence and location of continents would significantly influence the results shown here through the modulation of ocean circulations (Yang et al. 2019). Note, Leconte (2018) argued that tidally locked planets with emergent continents will tend to have their continents migrate to the substellar or antistellar points. If continents cluster near the substellar point, recent work with ROCKE-3D suggests that this would mute the effects of ocean circulations (Salazar et al. 2020). The varied location of continents remains a significant uncertainty in modern terrestrial exoplanet climate modeling, due to their tight coupling to ocean circulations, ocean heat transport, and ultimately climate.

5. CONCLUSIONS

A major focus of exoplanetary studies lies in the exploration of the full diversity of planetary system architectures. However, some of these architectures are similar enough to our own solar system such that they may shed insight into the orbital and atmospheric evolution of our terrestrial planets. Thus, systems that contain terrestrial planets within both the VZ and the HZ are of particular interest for the investigation of potential Venus/Earth analogs that exist within similar yet different contexts of age, composition, host star type, and orbital dynamics.

The Kepler-1649 system is one of the few known systems to harbor such a potential Venus/Earth analog, where the similar age and, presumably, composition of the planets allows the removal of several free parameters from which other comparative studies may be conducted. Here we have presented the results of dynamical analysis in which we have demonstrated that additional terrestrial planets could exist in orbits that lie between the two known planets. This is not an unlikely scenario given the dynamical packing observed for compact planetary systems (Fang & Margot 2013; Winn & Fabrycky

2015) and the necessity of coplanarity for transits to be observed (Fang & Margot 2012; Ballard & Johnson 2016). Additionally, the locations of significance resonance, such as the potential 3:2 MMR chain described in Section 2, lend credence to a possible planet located between the known b and c planets. Our dynamical simulations further demonstrate that varying eccentricity can be used as a tool to exclude either eccentricities of the known planets or the presence of the hypothetical additional planet. We also explored the effect of eccentricity on the dynamical evolution of the two known planets, the results of which show that the system is stable up to eccentricities of ~ 0.3 and that the frequency of the eccentricity oscillations can be exceptionally high (1000–3000 years). Such high-frequency eccentricity oscillations are a fundamental component of Milankovitch cycles for exoplanets (Deitrick et al. 2018a,b; Horner et al. 2020) and may play an important role in climate evolution.

Our ROCKE-3D simulations for the climate of Kepler-1649c under various eccentricity and ocean circulation assumptions demonstrate that in fact the surface temperature variation remains relatively small, even for eccentricity at the high end. The region of highest climate stability consistently lies in the substellar hemisphere for all of our simulations, indicating a potential longitude dependence of metabolic processes for any life that may exist on such a planet. Thus, the overall combination of both dynamical and climate evolution studies for this planetary system show that even though their orbits may change far more rapidly than that observed within the Solar System, atmospheric characterization may yet reveal robust environments that maintain temperate surface conditions. Such dynamically active systems should therefore not be ruled out in the continuing search for potentially habitable worlds.

ACKNOWLEDGEMENTS

The authors would like to thank Michael Way for valuable feedback on the climate simulation methodology, and the anonymous referee for the useful corrections. This research has made use of the Habitable Zone Gallery at hzzgallery.org. The results reported herein benefited from collaborations and/or information exchange within NASA’s Nexus for Exoplanet System Science (NExSS) research coordination network sponsored by NASA’s Science Mission Directorate.

Software: Mercury (Chambers 1999), REBOUND (Rein & Liu 2012), ROCKE-3D (Way et al. 2017)

REFERENCES

- Angelo, I., Rowe, J. F., Howell, S. B., et al. 2017, *AJ*, 153, 162, doi: [10.3847/1538-3881/aa615f](https://doi.org/10.3847/1538-3881/aa615f)
- Ballard, S., & Johnson, J. A. 2016, *ApJ*, 816, 66, doi: [10.3847/0004-637X/816/2/66](https://doi.org/10.3847/0004-637X/816/2/66)

- Barnes, R., Mullins, K., Goldblatt, C., et al. 2013, *Astrobiology*, 13, 225, doi: [10.1089/ast.2012.0851](https://doi.org/10.1089/ast.2012.0851)
- Batygin, K., & Morbidelli, A. 2013, *A&A*, 556, A28, doi: [10.1051/0004-6361/201220907](https://doi.org/10.1051/0004-6361/201220907)
- Borucki, W. J., Koch, D., Basri, G., et al. 2010, *Science*, 327, 977, doi: [10.1126/science.1185402](https://doi.org/10.1126/science.1185402)
- Boutle, I. A., Mayne, N. J., Drummond, B., et al. 2017, *A&A*, 601, A120, doi: [10.1051/0004-6361/201630020](https://doi.org/10.1051/0004-6361/201630020)
- Catanzarite, J., & Shao, M. 2011, *ApJ*, 738, 151, doi: [10.1088/0004-637X/738/2/151](https://doi.org/10.1088/0004-637X/738/2/151)
- Chambers, J. E. 1999, *MNRAS*, 304, 793, doi: [10.1046/j.1365-8711.1999.02379.x](https://doi.org/10.1046/j.1365-8711.1999.02379.x)
- Chambers, J. E., Wetherill, G. W., & Boss, A. P. 1996, *Icarus*, 119, 261, doi: [10.1006/icar.1996.0019](https://doi.org/10.1006/icar.1996.0019)
- Checlair, J. H., Olson, S. L., Jansen, M. F., & Abbot, D. S. 2019, *ApJL*, 884, L46, doi: [10.3847/2041-8213/ab487d](https://doi.org/10.3847/2041-8213/ab487d)
- Chen, J., & Kipping, D. 2017, *ApJ*, 834, 17, doi: [10.3847/1538-4357/834/1/17](https://doi.org/10.3847/1538-4357/834/1/17)
- Colose, C. M., Del Genio, A. D., & Way, M. J. 2019, *ApJ*, 884, 138, doi: [10.3847/1538-4357/ab4131](https://doi.org/10.3847/1538-4357/ab4131)
- Correia, A. C. M., & Laskar, J. 2004, *Nature*, 429, 848, doi: [10.1038/nature02609](https://doi.org/10.1038/nature02609)
- Deitrick, R., Barnes, R., Quinn, T. R., et al. 2018a, *AJ*, 155, 60, doi: [10.3847/1538-3881/aaa301](https://doi.org/10.3847/1538-3881/aaa301)
- Deitrick, R., Barnes, R., Bitz, C., et al. 2018b, *AJ*, 155, 266, doi: [10.3847/1538-3881/aac214](https://doi.org/10.3847/1538-3881/aac214)
- Del Genio, A. D., Way, M. J., Amundsen, D. S., et al. 2019, *Astrobiology*, 19, 99, doi: [10.1089/ast.2017.1760](https://doi.org/10.1089/ast.2017.1760)
- Dittmann, J. A., Irwin, J. M., Charbonneau, D., et al. 2017, *Nature*, 544, 333, doi: [10.1038/nature22055](https://doi.org/10.1038/nature22055)
- Dressing, C. D., & Charbonneau, D. 2015, *ApJ*, 807, 45, doi: [10.1088/0004-637X/807/1/45](https://doi.org/10.1088/0004-637X/807/1/45)
- Duncan, M. J., Levison, H. F., & Lee, M. H. 1998, *AJ*, 116, 2067, doi: [10.1086/300541](https://doi.org/10.1086/300541)
- Fang, J., & Margot, J.-L. 2012, *ApJ*, 761, 92, doi: [10.1088/0004-637X/761/2/92](https://doi.org/10.1088/0004-637X/761/2/92)
- . 2013, *ApJ*, 767, 115, doi: [10.1088/0004-637X/767/2/115](https://doi.org/10.1088/0004-637X/767/2/115)
- Faucher, T. J., Turbet, M., Wolf, E. T., et al. 2020, *Geoscientific Model Development*, 13, 707, doi: [10.5194/gmd-13-707-2020](https://doi.org/10.5194/gmd-13-707-2020)
- Fujii, Y., Del Genio, A. D., & Amundsen, D. S. 2017, *ApJ*, 848, 100, doi: [10.3847/1538-4357/aa8955](https://doi.org/10.3847/1538-4357/aa8955)
- Gillon, M., Jehin, E., Lederer, S. M., et al. 2016, *Nature*, 533, 221, doi: [10.1038/nature17448](https://doi.org/10.1038/nature17448)
- Gillon, M., Triaud, A. H. M. J., Demory, B.-O., et al. 2017, *Nature*, 542, 456, doi: [10.1038/nature21360](https://doi.org/10.1038/nature21360)
- Gladman, B. 1993, *Icarus*, 106, 247, doi: [10.1006/icar.1993.1169](https://doi.org/10.1006/icar.1993.1169)
- Hadden, S. 2019, *AJ*, 158, 238, doi: [10.3847/1538-3881/ab5287](https://doi.org/10.3847/1538-3881/ab5287)
- Hadden, S., & Lithwick, Y. 2018, *AJ*, 156, 95, doi: [10.3847/1538-3881/aad32c](https://doi.org/10.3847/1538-3881/aad32c)
- Haqq-Misra, J., Wolf, E. T., Joshi, M., Zhang, X., & Kopparapu, R. K. 2018, *ApJ*, 852, 67, doi: [10.3847/1538-4357/aa9f1f](https://doi.org/10.3847/1538-4357/aa9f1f)
- Hinse, T. C., Christou, A. A., Alvarelos, J. L. A., & Goździewski, K. 2010, *MNRAS*, 404, 837, doi: [10.1111/j.1365-2966.2010.16307.x](https://doi.org/10.1111/j.1365-2966.2010.16307.x)
- Horner, J., Vervoort, P., Kane, S. R., et al. 2020, *AJ*, 159, 10, doi: [10.3847/1538-3881/ab5365](https://doi.org/10.3847/1538-3881/ab5365)
- Kane, S. R. 2015, *ApJL*, 814, L9, doi: [10.1088/2041-8205/814/1/L9](https://doi.org/10.1088/2041-8205/814/1/L9)
- . 2016, *ApJ*, 830, 105, doi: [10.3847/0004-637X/830/2/105](https://doi.org/10.3847/0004-637X/830/2/105)
- . 2018, *ApJL*, 861, L21, doi: [10.3847/2041-8213/aad094](https://doi.org/10.3847/2041-8213/aad094)
- . 2019, *AJ*, 158, 72, doi: [10.3847/1538-3881/ab2a09](https://doi.org/10.3847/1538-3881/ab2a09)
- Kane, S. R., Ceja, A. Y., Way, M. J., & Quintana, E. V. 2018, *ApJ*, 869, 46, doi: [10.3847/1538-4357/aaec68](https://doi.org/10.3847/1538-4357/aaec68)
- Kane, S. R., Ciardi, D. R., Gelino, D. M., & von Braun, K. 2012, *MNRAS*, 425, 757, doi: [10.1111/j.1365-2966.2012.21627.x](https://doi.org/10.1111/j.1365-2966.2012.21627.x)
- Kane, S. R., & Gelino, D. M. 2012, *PASP*, 124, 323, doi: [10.1086/665271](https://doi.org/10.1086/665271)
- Kane, S. R., Kopparapu, R. K., & Domagal-Goldman, S. D. 2014, *ApJL*, 794, L5, doi: [10.1088/2041-8205/794/1/L5](https://doi.org/10.1088/2041-8205/794/1/L5)
- Kane, S. R., & Raymond, S. N. 2014, *ApJ*, 784, 104, doi: [10.1088/0004-637X/784/2/104](https://doi.org/10.1088/0004-637X/784/2/104)
- Kane, S. R., Turnbull, M. C., Fulton, B. J., et al. 2020a, *AJ*, 160, 81, doi: [10.3847/1538-3881/ab9ffe](https://doi.org/10.3847/1538-3881/ab9ffe)
- Kane, S. R., Vervoort, P., Horner, J., & Pozuelos, F. J. 2020b, *PSJ*, 1, 42, doi: [10.3847/PSJ/abae63](https://doi.org/10.3847/PSJ/abae63)
- Kane, S. R., Hill, M. L., Kasting, J. F., et al. 2016, *ApJ*, 830, 1, doi: [10.3847/0004-637X/830/1/1](https://doi.org/10.3847/0004-637X/830/1/1)
- Kane, S. R., Arney, G., Crisp, D., et al. 2019, *Journal of Geophysical Research (Planets)*, 124, 2015, doi: [10.1029/2019JE005939](https://doi.org/10.1029/2019JE005939)
- Kanodia, S., Wolfgang, A., Stefansson, G. K., Ning, B., & Mahadevan, S. 2019, *ApJ*, 882, 38, doi: [10.3847/1538-4357/ab334c](https://doi.org/10.3847/1538-4357/ab334c)
- Kasting, J. F., Whitmire, D. P., & Reynolds, R. T. 1993, *Icarus*, 101, 108, doi: [10.1006/icar.1993.1010](https://doi.org/10.1006/icar.1993.1010)
- Kopparapu, R. K. 2013, *ApJ*, 767, L8, doi: [10.1088/2041-8205/767/1/L8](https://doi.org/10.1088/2041-8205/767/1/L8)
- Kopparapu, R. K., & Barnes, R. 2010, *ApJ*, 716, 1336, doi: [10.1088/0004-637X/716/2/1336](https://doi.org/10.1088/0004-637X/716/2/1336)
- Kopparapu, R. K., Ramirez, R. M., SchottelKotte, J., et al. 2014, *ApJ*, 787, L29, doi: [10.1088/2041-8205/787/2/L29](https://doi.org/10.1088/2041-8205/787/2/L29)
- Kopparapu, R. k., Wolf, E. T., Arney, G., et al. 2017, *ApJ*, 845, 5, doi: [10.3847/1538-4357/aa7cf9](https://doi.org/10.3847/1538-4357/aa7cf9)
- Leconte, J. 2018, *Nature Geoscience*, 11, 168, doi: [10.1038/s41561-018-0071-2](https://doi.org/10.1038/s41561-018-0071-2)

- Luger, R., Sestovic, M., Kruse, E., et al. 2017, *Nature Astronomy*, 1, 0129, doi: [10.1038/s41550-017-0129](https://doi.org/10.1038/s41550-017-0129)
- Ment, K., Dittmann, J. A., Astudillo-Defru, N., et al. 2019, *AJ*, 157, 32, doi: [10.3847/1538-3881/aaf1b1](https://doi.org/10.3847/1538-3881/aaf1b1)
- Millholland, S., Wang, S., & Laughlin, G. 2017, *ApJL*, 849, L33, doi: [10.3847/2041-8213/aa9714](https://doi.org/10.3847/2041-8213/aa9714)
- Neil, A. R., & Rogers, L. A. 2020, *ApJ*, 891, 12, doi: [10.3847/1538-4357/ab6a92](https://doi.org/10.3847/1538-4357/ab6a92)
- Olson, S. L., Jansen, M., & Abbot, D. S. 2020, *ApJ*, 895, 19, doi: [10.3847/1538-4357/ab88c9](https://doi.org/10.3847/1538-4357/ab88c9)
- Ostberg, C., & Kane, S. R. 2019, *AJ*, 158, 195, doi: [10.3847/1538-3881/ab44b0](https://doi.org/10.3847/1538-3881/ab44b0)
- Otegi, J. F., Bouchy, F., & Helled, R. 2020, *A&A*, 634, A43, doi: [10.1051/0004-6361/201936482](https://doi.org/10.1051/0004-6361/201936482)
- Petrovich, C. 2015, *ApJ*, 808, 120, doi: [10.1088/0004-637X/808/2/120](https://doi.org/10.1088/0004-637X/808/2/120)
- Pierrehumbert, R. T. 2011, *ApJL*, 726, L8, doi: [10.1088/2041-8205/726/1/L8](https://doi.org/10.1088/2041-8205/726/1/L8)
- Quintana, E. V., Barclay, T., Raymond, S. N., et al. 2014, *Science*, 344, 277, doi: [10.1126/science.1249403](https://doi.org/10.1126/science.1249403)
- Rein, H., & Liu, S. F. 2012, *A&A*, 537, A128, doi: [10.1051/0004-6361/201118085](https://doi.org/10.1051/0004-6361/201118085)
- Rein, H., & Tamayo, D. 2015, *MNRAS*, 452, 376, doi: [10.1093/mnras/stv1257](https://doi.org/10.1093/mnras/stv1257)
- Salazar, A. M., Olson, S. L., Komacek, T. D., Stephens, H., & Abbot, D. S. 2020, *ApJL*, 896, L16, doi: [10.3847/2041-8213/ab94c1](https://doi.org/10.3847/2041-8213/ab94c1)
- Smith, A. W., & Lissauer, J. J. 2009, *Icarus*, 201, 381, doi: [10.1016/j.icarus.2008.12.027](https://doi.org/10.1016/j.icarus.2008.12.027)
- Spalding, C., Marx, N. W., & Batygin, K. 2018, *AJ*, 155, 167, doi: [10.3847/1538-3881/aab43a](https://doi.org/10.3847/1538-3881/aab43a)
- Turbet, M., Bolmont, E., Ehrenreich, D., et al. 2020, *A&A*, 638, A41, doi: [10.1051/0004-6361/201937151](https://doi.org/10.1051/0004-6361/201937151)
- Turbet, M., Leconte, J., Selsis, F., et al. 2016, *A&A*, 596, A112, doi: [10.1051/0004-6361/201629577](https://doi.org/10.1051/0004-6361/201629577)
- Vanderburg, A., Rowden, P., Bryson, S., et al. 2020, *ApJL*, 893, L27, doi: [10.3847/2041-8213/ab84e5](https://doi.org/10.3847/2041-8213/ab84e5)
- Vinson, B. R., & Chiang, E. 2018, *MNRAS*, 474, 4855, doi: [10.1093/mnras/stx3091](https://doi.org/10.1093/mnras/stx3091)
- Way, M. J., Del Genio, A. D., Aleinov, I., et al. 2018, *ApJS*, 239, 24, doi: [10.3847/1538-4365/aae9e1](https://doi.org/10.3847/1538-4365/aae9e1)
- Way, M. J., & Georgakarakos, N. 2017, *ApJ*, 835, L1, doi: [10.3847/2041-8213/835/1/L1](https://doi.org/10.3847/2041-8213/835/1/L1)
- Way, M. J., Aleinov, I., Amundsen, D. S., et al. 2017, *ApJS*, 231, 12, doi: [10.3847/1538-4365/aa7a06](https://doi.org/10.3847/1538-4365/aa7a06)
- Weiss, L. M., Marcy, G. W., Petigura, E. A., et al. 2018, *AJ*, 155, 48, doi: [10.3847/1538-3881/aa9ff6](https://doi.org/10.3847/1538-3881/aa9ff6)
- Winn, J. N., & Fabrycky, D. C. 2015, *ARA&A*, 53, 409, doi: [10.1146/annurev-astro-082214-122246](https://doi.org/10.1146/annurev-astro-082214-122246)
- Wisdom, J. 2006, *AJ*, 131, 2294, doi: [10.1086/500829](https://doi.org/10.1086/500829)
- Wisdom, J., & Holman, M. 1991, *AJ*, 102, 1528, doi: [10.1086/115978](https://doi.org/10.1086/115978)
- Yang, J., Abbot, D. S., Koll, D. D. B., Hu, Y., & Showman, A. P. 2019, *ApJ*, 871, 29, doi: [10.3847/1538-4357/aaf1a8](https://doi.org/10.3847/1538-4357/aaf1a8)
- Zeng, L., Jacobsen, S. B., Sasselov, D. D., et al. 2019, *Proceedings of the National Academy of Science*, 116, 9723, doi: [10.1073/pnas.1812905116](https://doi.org/10.1073/pnas.1812905116)